Available online at www.sciencedirect.com
SCIENCE DIRECT®
International Journal of Heat and Mass Transfer 49 (2006) 63–77
International Journal of HEAT and MASS TRANSFER
www.elsevier.com/locate/ijhmt

Effectiveness of energy wheels from transient measurements: Part II—Results and verification

O.O. Abe, C.J. Simonson *, R.W. Besant, W. Shang

Department of Mechanical Engineering, University of Saskatchewan, 57 Campus Drive, Saskatoon, SK, Canada S7N 5A9

Received 15 June 2005; received in revised form 5 August 2005
Available online 13 October 2005

Abstract

This paper verifies the accuracy of a new transient test method for air-to-air energy wheels. To accomplish this, the transient characteristics of several energy wheels exposed to separate and independent step changes in humidity and temperature are measured. These characteristics are then used to predict the effectiveness of the wheels using the effectiveness model presented in Part I of this paper [O.O. Abe, C.J. Simonson, R.W. Besant and W. Shang, Effectiveness of energy wheels from transient measurements: Part I—Prediction of effectiveness and uncertainty, Int. J. Heat Mass Transfer, accepted for publication. [1]]. Comparison of the predicted latent and sensible effectiveness with experimental standard test data (steady state) show agreement within uncertainty bounds. Comparison with numerical simulations results also show agreement within the uncertainty bounds except for the special case of very low face velocity entering the energy wheels.

Keywords: Transient; Humidity; Temperature; Time constant; Effectiveness; Energy wheel

1. Introduction

Two inlet conditions (ARI summer (hot humid) and winter (cold dry) conditions) are used to certify the performance of air-to-air recovery devices as specified in [2]. Since large variations in the ambient air conditions occur over the year, HVAC design engineers need to be concerned with optimization of their designs to improve indoor air quality, while reducing the HVAC system capital and operating costs to a minimum. Often this implies the use of energy wheels for heat and moisture exchange between supply and exhaust airflows. Therefore, the testing of energy wheels is very important to determine and check the performance according to their design optimization. There are many factors that must be considered to fully test or characterize the performance of an energy wheel. These factors include the: sensible, latent and total effectiveness, outside air correction factor for the supply air delivered, exhaust air transfer ratio and air pressure drop across the wheel for both the supply and exhaust airflows through the wheel [2,3]. Certification testing using these standards for many types and sizes of wheels produced by each manufacturer has proven to be expensive and time consuming if the uncertainties are limited within specified bounds. These facts have motivated this research. A new transient test method is proposed to determine the effectiveness of energy wheels with closed flow channels. This test method only

* Corresponding author. Tel.: +1 306 966 5479; fax: +1 306 966 5427.
E-mail address: Carey.Simonson@usask.ca (C.J. Simonson).

0017-9310/$ - see front matter © 2005 Elsevier Ltd. All rights reserved.
doi:10.1016/j.ijheatmasstransfer.2005.08.009

Nomenclature

HVAC	heating, ventilating and air conditioning
MS-100	100-mm thick energy wheel coated with molecular sieve desiccant
MS-200	200-mm thick energy wheel coated with molecular sieve desiccant
NTU	number of transfer units
RH	relative humidity
rpm	revolutions per minute
SG-150	150-mm thick energy wheel coated with silica gel desiccant
T	bulk temperature (°C or K)
$U(\eta)$	uncertainty in parameter η
V_{air}	face velocity of the wheel (m/s)
5% D	an energy wheel with 5% desiccant by mass
10% D	an energy wheel with 10% desiccant by mass
20% D	an energy wheel with 20% desiccant by mass

Greek symbols

Δ	difference
ε	effectiveness
τ	time constant
Φ	general variable (relative humidity or temperature)
ϕ	relative humidity
χ	weighting factor

Subscripts

ads	adsorption
des	desorption
f	final
i	initial
l	latent
s	sensible
i,c	inlet cold side
i,h	inlet hot side
i,d	inlet dry side
i,w	inlet wet side
o,c	outlet cold side
o,h	outlet hot side
o,d	outlet dry side
o,w	outlet wet side

requires the use of a small experimental apparatus that is able to get performance data rapidly [4].

There have been several research papers on the humidity and temperature response of heat and moisture exchangers when these exchangers are subjected to a step change in inlet operating conditions [4–9]. A number of researchers have also used transient testing techniques to determine the convective heat transfer coefficient between the heat transfer surface of the core and the fluid from the temperature–time history of the fluid leaving the core [10–12]. However, there are no research papers on the prediction of the effectiveness of those exchangers using transient data.

During the normal operation of energy wheels, the matrix undergoes a periodic step change in input conditions as the wheel rotates between the cold and warm airflows. It is hypothesized that it will be possible to predict the effectiveness of an energy wheel using only data obtained during a single step response from a transient test. Therefore, the objectives of this paper are to: (1) use the transient test facility developed by [4] and shown in Fig. 1 to measure the transient characteristics (i.e., time constants) of several non-rotating wheels exposed to step changes in humidity and temperature; (2) determine the latent and sensible effectiveness of these wheels from the measured transient characteristics using the effectiveness model developed in Part I [1]; and (3) compare the effectiveness obtained with this new transient method with the results obtained from steady state experiments and numerical simulations.

2. Test facility and instrumentation

Fig. 1 shows a schematic of the test apparatus and instrumentation for measuring the transient response characteristics of sensors and energy wheels. The facility provides two air streams with well controlled properties (flow rate (±0.03 L/s), temperature (±0.5 °C) and relative humidity (±1% RH)) to a test section where the sensors and energy wheels will be tested. The mass flow rate of air entering the test section is controlled with a mass flow controller, the temperature is controlled with the heat exchanger and the humidity is maintained using the dryer and the three water tanks shown in Fig. 1(a). When testing the thermal response of sensors and wheels, the two inlet air streams are both dry (~4% RH) but have different temperatures. In this paper, one air stream will be maintained at room temperature (~23 °C), while the other air stream will be maintained at 50 °C for one test and 44 °C for another test. When testing the transient moisture response, the two inlet air streams have the same temperature (~23 °C), but have different humidities—one at 4% RH and the other at 40%, 50% or 60% RH. These different conditions will show the impact of operating conditions on the transient response of sensors and wheels. In addition to the different temperature and humidity conditions, two different air flow rates will be studied (3.3 and 1.7 L/s giving average velocities in the 51 mm inside diameter tubes of 1.6 and 0.8 m/s). These different face velocities are chosen to correspond with the face veloc-

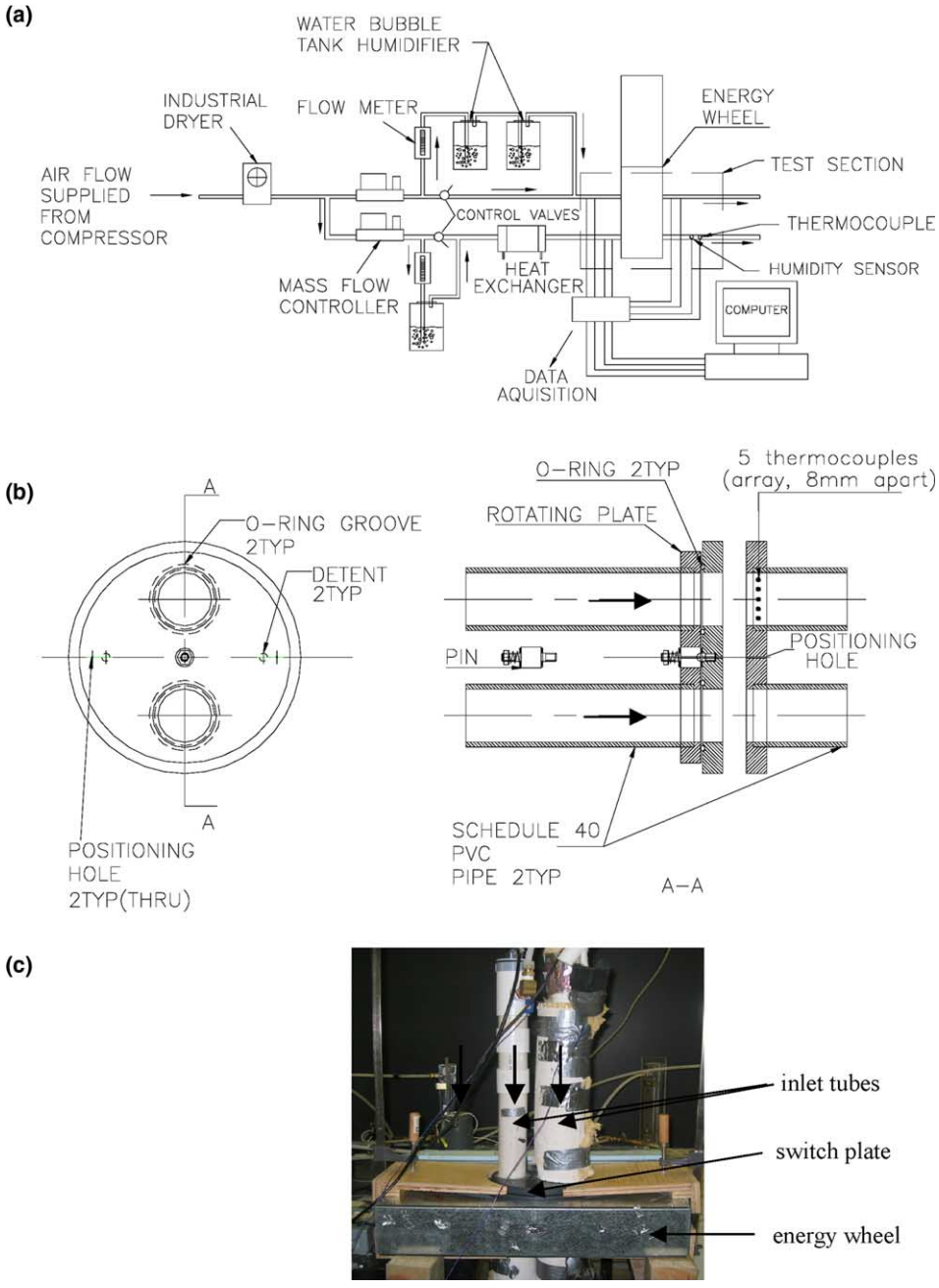

Fig. 1. Schematics of the test facility showing (a) the flow lines, instrumentation and test wheel (b) flow tube and (c) the test section with its rapid tube rotation capability between the two inlet flow tubes.

ities used to test energy wheels using the standard steady state method [13].

The step changes in humidity and temperature are achieved by manually rotating the two inlet tubes 180°. The inlet flow tubes are attached to a rotary switch plate which can be rotated 180° with respect to the outlet flow tubes as shown in Fig. 1(b). These step changes take less than one second for the air flow properties to completely change. Fig. 1(c) shows a picture of the test section, clamped on to a stationary energy wheel. Insulation is used to minimize heat transfer from the hot air to the ambient air. In addition, an array of equally spaced thermocouples is installed (shown in Fig. 1(b)) inside one of the outlet insulated tubes so that the

temperature profile across the tube diameter can be measured. The apparatus in Fig. 1 is significantly different from the standard test facility specified in [3]. This standard state test method uses a counter airflow configuration through rotating energy wheels, while the transient test equipment shown in Fig. 1 uses a parallel airflow configuration with both airflows in the same direction through a stationary energy wheel. Furthermore, the transient test facility does not require large and expensive chillers, boilers and fans as required in the standard test facility when testing large exchangers. It is anticipated that this test facility could readily be adapted into manufacturing plants for quality control or applied when field testing installed energy wheels.

2.1. Steady state calibration of instruments

2.1.1. Humidity measurement

The four thin-film polymer humidity sensors used in the facility measure the relative humidity of the two air streams as the air enters and leaves the test section. Although this instrument can also measure temperature using a RTD (resistance thermal device) temperature sensor, it is not used to measure temperature in this investigation because this RTD sensor has a very slow thermal response [14,15]. In this paper, the instrument is used to measure relative humidity only under constant temperature conditions. For these conditions, the humidity sensors were calibrated against a chilled mirror sensor with a bias uncertainty of ±0.3 °C in dew point and ±1% RH at 20 °C and the resulting bias in the calibrated humidity sensor is ±1.8% RH at room temperature. The transient response of the humidity sensors is also important for this transient investigation as described in [4,14]. These studies used the same sensors as used in this paper and showed that these humidity sensors correlate well with exponential functions having two time constants. The general exponential equation for any variable (Φ) following a step increase of $\Delta\Phi_0$ is

$$\frac{\Delta\Phi}{\Delta\Phi_0} = \chi_1(1 - e^{-t/\tau_1}) + \chi_2(1 - e^{-t/\tau_2}) \quad (1)$$

and for a step decrease of $\Delta\Phi$ the equation is

$$\frac{\Delta\Phi}{\Delta\Phi_0} = \chi_1 e^{-t/\tau_1} + \chi_2 e^{-t/\tau_2} \quad (2)$$

where the weighting factors χ_1 and χ_2 satisfy the equation

$$\chi_1 + \chi_2 = 1, \quad \chi_1 \geqslant 0, \quad \chi_2 \geqslant 0 \quad (3)$$

but with different values of χ_1 and χ_2 for each experiment. Other variables include:

$\Delta\Phi$ measured change in the general variable (temperature or relative humidity) $= |\Phi - \Phi_i|$, where Φ_i is the initial value;

$\Delta\Phi_0$ maximum step change in the general variable (temperature or relative humidity) $= |\Phi_f - \Phi_i|$, where Φ_f is the final value;

τ_1, τ_2 the first and second time constants respectively.

For the humidity sensors in this paper following a step increase in humidity (i.e., during absorption of water vapour in the sensor), the coefficients in Eq. (1) are $\chi_1 = 0.91$, $\tau_1 = 3.1$ s, $\chi_2 = 0.09$ and $\tau_2 = 90$ s [4,14]. In Eq. (2) (i.e., during desorption), the coefficients are $\chi_1 = 0.97$, $\tau_1 = 2.6$ s, $\chi_2 = 0.03$ and $\tau_2 = 290$ s [4,14]. These characteristics quantify the transient response of the humidity sensors and will be used to analyse the results in this paper.

2.1.2. Temperature measurement

The air temperature is measured using T-type thermocouples. The thermocouples used were calibrated at steady state against a standard calibrator with an accuracy of ±0.1 °C over a wide range of temperatures. After calibration, the bias uncertainty in the T-type thermocouples was determined to be ±0.2 °C for all the thermocouples used. As with the humidity sensors, the transient characteristics of the thermocouples can be correlated using Eqs. (1) and (2). These transient characteristics of the thermocouples used in this paper have been measured by [14–16] to be $\chi_1 = 0.76$, $\tau_1 = 5.1$ s, $\chi_2 = 0.24$ and $\tau_2 = 130$ s for an increase in temperature (Eq. (1)) and $\chi_1 = 0.8$, $\tau_1 = 5.1$ s, $\chi_2 = 0.2$ and $\tau_2 = 160$ s for a decrease in temperature (Eq. (2)).

3. Transient response experiments on energy wheels

In this section, the results of transient response experiments are presented for three different wheels with effectiveness and uncertainty values that have been determined using the standard steady state testing method [3,13]. The energy wheels will be named according to their thickness and desiccant coating. MS-100 is a 100-mm thick energy wheel coated with molecular sieve desiccant. SG-150 is a 150-mm thick energy wheel coated with silica gel desiccant. MS-200 is a 200-mm thick energy wheel coated with molecular sieve desiccant. These designations are used throughout the paper. The face velocity used to test each wheel will correspond to the velocities used by [13]. The experimental test facility shown in Fig. 1 is used to measure the transient response characteristics of energy wheels for both a step change in the inlet flow humidity or temperature when humidity sensors and thermocouples are placed upstream and downstream of the wheel. Since the response of the energy wheel measured in this way includes both the characteristics of the sensor and wheel, it is necessary to deconvolute the response of the wheel

alone from the measured response of the wheel plus sensor. The analysis of [4,14] will be used for this purpose. Once the characteristics (i.e., weighting factors and time constants in Eqs. (1) and (2)) of the wheel alone are known, the effectiveness of the wheel can be predicted using the model presented in Part I of this paper [1].

The experimental apparatus shown in Fig. 1 is designed to obtain the latent effectiveness using data from the transient response characteristics of an energy wheel plus humidity sensor following a step change in inlet humidity. Similarly, the sensible effectiveness is obtained using data from the energy wheel plus thermocouple following a step change in inlet temperature. Before the start of each transient test, the test facility is run till steady state conditions are reached for all properties. Each transient test is started when the inlet conditions of the supply air tubes entering a stationary wheel are interchanged in a step fashion and the outlet sensors (humidity sensors or thermocouples) undergo a decrease or increase in either the humidity or temperature. During this step change the stationary wheel matrix gains or loses either moisture or heat until the test is completed. Each test is completed when these outlet sensor readings approach the inlet conditions after about 30 min.

As noted previously, the humidity and temperature response of energy wheels are tested independently. The humidity transient response experiments are performed under isothermal inlet airflow conditions so that heat transfer effects are negligible. The temperature transient response experiments are performed under dry test conditions where there is negligible moisture transfer.

3.1. Energy wheel plus humidity sensor tests

Fig. 2 shows the measured energy wheel plus humidity sensor response data for two different energy wheels experiencing a step change in inlet humidity from 5% RH to 40% RH at about 50 s with both inlets at the same temperature (~23 °C). The face velocity is 1.6 m/s and the desiccant coating is a molecular sieve desiccant for both wheels. The only difference between the two wheels is the thickness of the wheel, which is 100 mm in Fig. 2(a) and 200 mm in Fig. 2(b). Fig. 2(b) shows a slower response compared to Fig. 2(a) because of the thickness of the wheel. Fig. 2 shows that the data from each outlet humidity sensors ($RH_{o,d}$ and $RH_{o,w}$) will correlate with an exponential type of equation with time after the step change. Wang et al. [4] found that the response of an energy wheel plus humidity sensor following a step change in humidity did not correlate well with only one time constant; therefore, the two-time constant correlations of Eqs. (1) and (2) are used for each outlet humidity increase and decrease. Eqs. (1) and (2) are found to result in good correlations when the best-fit values of the empirical weighting factors (χ_1, χ_2) and time constants (τ_1, τ_2) are chosen.

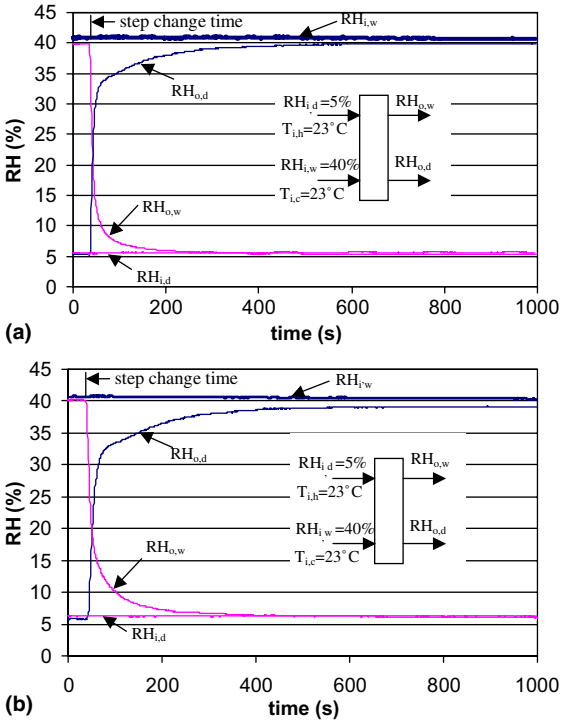

Fig. 2. Measured inlet and outlet relative humidities for (a) 100 mm and (b) 200-mm thick energy wheel with molecular sieve coated wheel matrix exposed to a step change in relative humidity with no change in temperature ($\Delta RH = 35\%$, $\Delta T = 0$).

Table 1 lists the characteristic coefficients obtained using a commercial software package and the correlation Eqs. (1) and (2) for the different wheel plus humidity sensor experiments on the 100-mm thick wheel coated with a molecular sieve desiccant (MS-100). The data are correlated using 30 min of data where each sensor reading is recorded every second, giving 1800 data points. The r^2 curve fit correlation parameter is defined as the goodness of curve fit; it indicates how well correlation data agrees with the experimental data. For all the tests summarized in Table 1, r^2 has a range $0.974 < r^2 < 0.997$ indicating good fits. Note that when χ_2 is set equal to zero the resulting r^2 is only $0.876 < r^2 < 0.899$ indicating a poor correlation.

The data in Table 1 shows that the first time constant is the most important because the first weighting factor is several times larger than the second weighting factor. The first time constant is thought to be mostly due to the diffusion of water vapour to or from the surface of the wheel matrix and adsorption or desorption on the outer surface of the desiccant particles in the wheel matrix coating. The second time constant, with a correspondingly small weighting factor, was at least an order of magnitude greater than the first time constant. This

Table 1
Water vapour adsorption and desorption coefficients (χ_1, χ_2) and time constants (τ_1, τ_2) in Eqs. (1) and (2) for Wheel MS-100 plus humidity sensor with $\Delta RH \neq 0$, $\Delta T = 0$, $V_{air} = 1.6$ m/s for three different humidity step sizes

Inlet conditions	χ_1	τ_1 (s)	χ_2	τ_1 (s)	r^2
Adsorption (Eq. (1))					
Dry side: $T_{i,d} \approx 23$ °C, $\phi_{i,d} \approx 5\%$	0.80	8.3	0.20	133.7	0.983
Wet side: $T_{i,w} \approx 23$ °C, $\phi_{i,w} \approx 40\%$	0.82	11.2	0.18	146.3	0.992
	0.84	12.1	0.16	152.8	0.979
Dry side: $T_{i,d} \approx 23$ °C, $\phi_{i,d} \approx 5\%$	0.76	7.9	0.24	137.4	0.983
Wet side: $T_{i,w} \approx 23$ °C, $\phi_{i,w} \approx 50\%$	0.77	10.8	0.23	154.4	0.984
	0.82	6.7	0.18	123.4	0.984
Dry side: $T_{i,d} \approx 23$ °C, $\phi_{i,d} \approx 5\%$	0.79	9.7	0.21	139.1	0.982
Wet side: $T_{i,w} \approx 23$ °C, $\phi_{i,w} \approx 60\%$	0.81	6.9	0.19	118.4	0.981
	0.78	9.4	0.22	132.4	0.980
Desorption (Eq. (2))					
Dry side: $T_{i,d} \approx 23$ °C, $\phi_{i,d} \approx 5\%$	0.84	9.1	0.16	146.9	0.987
Wet side: $T_{i,w} \approx 23$ °C, $\phi_{i,w} \approx 40\%$	0.85	7.3	0.15	116.8	0.989
	0.82	8.3	0.18	140.4	0.986
Dry side: $T_{i,d} \approx 23$ °C, $\phi_{i,d} \approx 5\%$	0.92	9.5	0.08	188.8	0.986
Wet side: $T_{i,w} \approx 23$ °C, $\phi_{i,w} \approx 50\%$	0.79	7.2	0.21	131.2	0.986
	0.89	7.2	0.11	93.5	0.993
Dry side: $T_{i,d} \approx 23$ °C, $\phi_{i,d} \approx 5\%$	0.81	6.1	0.19	104.1	0.989
Wet side: $T_{i,w} \approx 23$ °C, $\phi_{i,w} \approx 60\%$	0.84	7.8	0.16	133.8	0.989
	0.81	6.3	0.19	107.5	0.985

second time constant is thought to be mostly a consequence of the slow diffusion process of water molecules into the inner regions of the desiccant particles in the coating of the wheel matrix and the sensor material as the wheel and sensor approach equilibrium.

Three different positions on the surface of each wheel are tested resulting in nine step change response tests for each wheel. The results for Wheel MS-100 in Table 1 show that the variations in the characteristic coefficients (χ_1, χ_2, τ_1 and τ_2) vary in a random manner for the three positions and two step changes (i.e., adsorption and desorption). Ref. [16] shows that the same is true for the other wheels except for the wheel with a silica gel coating (i.e., Wheel SG-150), where it is found that the time constant τ_1 tends to increase with increasing humidity step size for the desorption process. Since this effect is small for the Wheel SG-150, the coefficients (χ_1, χ_2, τ_1 and τ_2) for the wheels plus humidity sensor for both adsorption and desorption processes are statistically averaged for Gaussian distribution weighted according to the standard deviation of each coefficient [17].

The statistical average and the uncertainty calculated using 95% confidence limits for all the three wheels are presented in Table 2. Comparing values in Table 2, it is seen that the coefficients change for each wheel. This change reflects the thickness of each wheel and the type of desiccant. Comparing Wheels MS-100 and MS-200, which have different thickness but both have a molecular

Table 2
Average water vapour adsorption and desorption transient coefficients for three tested wheels plus humidity sensor

Process	$\overline{\chi_1} \pm U(\overline{\chi_1})$	$\overline{\tau_1} \pm U(\overline{\tau_1})$ (s)	$\overline{\chi_2} \pm U(\overline{\chi_2})$	$\overline{\tau_2} \pm U(\overline{\tau_2})$ (s)
Wheel MS-100 plus humidity sensor (V_{air} = 1.6 m/s)				
Adsorption	0.80 ± 0.02	10 ± 1	0.20 ± 0.02	138 ± 12
Desorption	0.84 ± 0.02	8 ± 1	0.16 ± 0.02	129 ± 21
Wheel SG-150 plus humidity sensor (V_{air} = 0.8 m/s)				
Adsorption	0.88 ± 0.04	14 ± 1	0.12 ± 0.04	181 ± 20
Desorption	0.95 ± 0.01	20 ± 3	0.05 ± 0.01	384 ± 72
Wheel MS-200 plus humidity sensor (V_{air} = 1.6 m/s)				
Adsorption	0.77 ± 0.02	17 ± 2	0.23 ± 0.02	166 ± 16
Desorption	0.84 ± 0.02	14 ± 1	0.16 ± 0.02	139 ± 25

sieve desiccant coating and are tested at the same face velocity of 1.6 m/s, the effect of wheel thickness is shown on the time constants. The thicker wheel has larger moisture transfer area and thus larger time constants. Wheel SG-150 differs from the other two wheels because it has a silica gel desiccant coating and is tested at a face velocity of 0.8 m/s. These different face velocities are chosen so that the transient effectiveness data can be directly compared with the steady-state effectiveness data of [13].

3.2. Energy wheel plus thermocouple tests

The purpose of this section is to determine the transient response characteristics of the same three wheels following a step change in the inlet temperatures using thermocouples located upstream and downstream of the wheel. Fig. 3 shows the measured temperature data for the (a) MS-100 and (b) MS-200 energy wheel experiencing a step change in inlet temperature from 23 °C to 50 °C but with no change in humidity conditions. Dry inlet air conditions are chosen (~4% RH) to minimize any effects due to moisture transfer. The temperature at the outlet is the bulk temperature weighted by the mass flow rate flowing through the area represented by each of the five thermocouples in the outlet tube shown in Fig. 1(b).

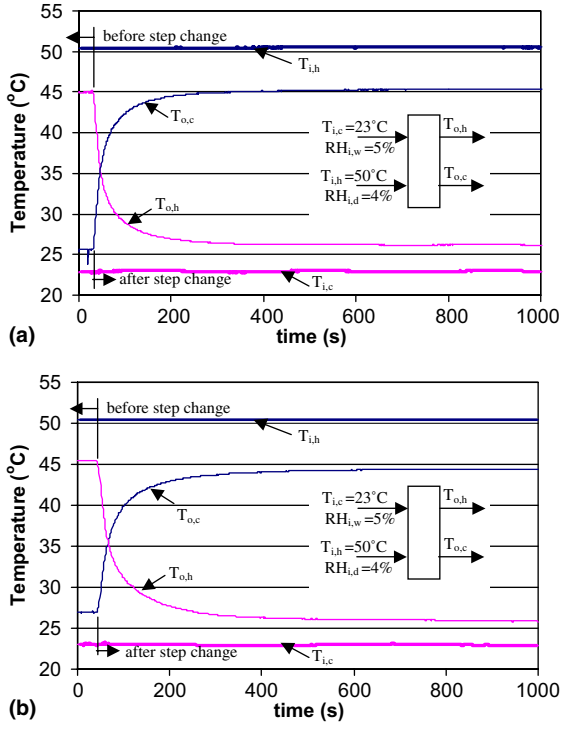

Fig. 3. Measured inlet and outlet temperatures for (a) Wheel MS-100 and (b) Wheel MS-200 exposed to a step change in temperature with no change in relative humidity ($\Delta T = 27$ °C, $\Delta RH = 0$).

In the transient response experiments for step changes in temperature shown in Fig. 3 there appears to be a very significant heat conduction effect through the wheel matrix because the outlet temperatures do not equal the inlet temperatures at steady state. Heat conduction effects are evident both before and after the step change in inlet conditions. Since the small area of the wheel being tested is not thermally isolated from the surrounding wheel matrix, there will be heat transfer between the matrix tubes with air flow and the surrounding tubes of the wheel which have no airflow. The effect of this lateral conduction between the part of the wheel being tested and the rest of the wheel has been investigated in detail by [15,16]. They present the measured temperature distributions in the outlet tubes which show a 0.5 °C variation between the 5 thermocouples in the outlet of the hot air stream and a 2 °C variation in the outlet of the cold airstream. These distributions indicate that the hot airstream is losing heat from its perimeter because it is surrounded by a large wheel that acts like an infinite body at room temperature, while the cold airstream is only gaining heat from the portion of the wheel that is heated by the hot airstream. The data in Fig. 3 confirm that the hot airstream loses more heat than the cold airstream gains because the temperature difference between $T_{i,h}$ and $T_{o,h}$ is larger than the difference between $T_{i,c}$ and $T_{o,c}$ before the time of the step change. Similarly, the difference between $T_{i,h}$ and $T_{o,c}$ is larger than the difference between $T_{i,c}$ and $T_{o,h}$ after the step change.

To investigate the effect of this heat conduction in the wheel matrix on the time constants of the wheel, Refs. [15,16] used the analytical solution of [18] which is for an adiabatic tube with no lateral heat conduction. They found that when the measured outlet temperatures are normalized by the maximum change in the experimental data (as used in Eqs. (1) and (2)), the first time constant obtained from the transient experimental data and analytical solution agree within the experimental and analytical uncertainty bounds as shown in Fig. 4. Therefore, in this paper, the normalized temperature will be correlated using Eqs. (1) and (2) to determine the characteristics of the energy wheel plus thermocouple for both temperature increases and decreases. The characteristic coefficients for Wheel MS-100 are listed in Table 3 and show that the first time constant is the most important and the second time constant is at least an order of magnitude greater than the first time constant. The second time constant is mostly a consequence of the slow heat diffusion process into the surrounding wheel matrix. For the coefficients in Table 3 and also for other two wheels, r^2 has a range $0.990 < r^2 < 0.999$ indicating good fits. It should be noted that when χ_2 is set equal to zero, the resulting r^2 values reduce to about 0.92.

The data in Table 3 show that there is no significant change in the characteristic coefficients (χ_1, χ_2, τ_1 and τ_2)

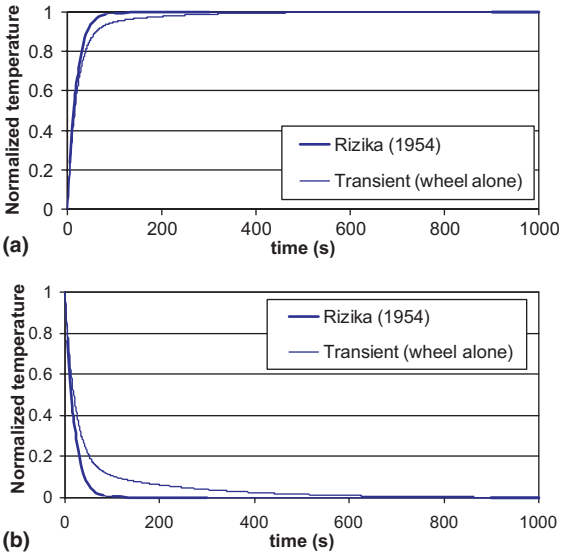

Fig. 4. Comparison of the normalized temperature transient response of Wheel MS-100 alone and the analytical solution of Rizika [18] for a (a) step increase in temperature (heating) and (b) step decrease in temperature (cooling).

for the wheel as the size of the temperature step changes. Also for tests conducted on the other two wheels (Wheels SG-150 and MS-200), there is no significant change in the characteristic coefficients as the temperature step sizes change. Table 4 presents the statistically averaged characteristic coefficients of the wheels plus thermocouple tests. Comparing values in the table, it is seen that these coefficients represent the characteristic properties of each wheel. The coefficients vary for each wheel depending on the size, face velocity and the type of desiccant, of each wheel. However, the data shows that the time constants of Wheel SG-150 are larger than those for Wheels MS-100 and MS-200. It is expected that the time constants of Wheel SG-150 and MS-200 will be larger than that of Wheel MS-100 because of the thickness (i.e., size) of the wheels and the results in Table 4 show this to be the case. Similarly, it may be expected that the time constants of Wheel SG-150 would be smaller than those of Wheel MS-200 because of the sizes of these wheels, but the reverse is the case as shown in Table 4. This is because the face velocities at which these coefficients are determined are not the same for both wheels. The coefficients of Wheel SG-150 are determined at a face velocity of 0.8 m/s while the coefficients of Wheel MS-200 are determined at 1.6 m/s. At a lower face velocity, the response of the wheel is slower (i.e., the time constants are larger). It is reminded that these different face velocities are chosen to correspond to the face velocity used in the steady state effectiveness measurements of [13].

3.3. Characteristic of the energy wheels alone

The transient response characteristics and correlation equations discussed in the previous Sections 3.1 and 3.2

Table 3
Heat transfer heating and cooling coefficients (χ_1, χ_2) and time constants (τ_1, τ_2) in Eqs. (1) and (2) for Wheel MS-100 plus thermocouple with $\Delta T \neq 0$, $\Delta RH = 0$, $V_{air} = 1.6$ m/s

Inlet conditions	χ_1	τ_1 (s)	χ_2	τ_1 (s)	r^2
Temperature increase (heating) (Eq. (1))					
Hot side: $T_{i,d} \approx 23$ °C, $\phi_{i,d} \approx 4\%$	0.88	27.1	0.12	429.8	0.993
Cold side: $T_{i,w} \approx 53$ °C, $\phi_{i,w} \approx 4\%$	0.83	20.2	0.17	124.8	0.995
	0.80	20.5	0.20	134.6	0.997
	0.79	22.3	0.11	146.7	0.997
	0.86	23.7	0.14	216.4	0.995
Hot side: $T_{i,d} \approx 23$ °C, $\phi_{i,d} \approx 4\%$	0.85	22.5	0.15	188.6	0.996
Cold side: $T_{i,w} \approx 44$ °C, $\phi_{i,w} \approx 4\%$	0.79	20.0	0.21	121.8	0.997
	0.79	19.9	0.21	122.6	0.998
	0.84	19.7	0.16	110.9	0.997
Temperature decrease (cooling) (Eq. (2))					
Hot side: $T_{i,d} \approx 23$ °C, $\phi_{i,d} \approx 4\%$	0.84	22.0	0.16	167.0	0.992
Cold side: $T_{i,w} \approx 53$ °C, $\phi_{i,w} \approx 4\%$	0.83	21.9	0.17	229.4	0.990
	0.79	19.6	0.21	122.2	0.995
	0.81	21.2	0.19	144.0	0.993
	0.82	21.4	0.18	145.3	0.994
Hot side: $T_{i,d} \approx 23$ °C, $\phi_{i,d} \approx 4\%$	0.84	19.1	0.16	132.0	0.995
Cold side: $T_{i,w} \approx 44$ °C, $\phi_{i,w} \approx 4\%$	0.81	20.2	0.19	127.1	0.993
	0.78	18.2	0.22	113.5	0.994
	0.81	19.2	0.19	111.4	0.994

Table 4
Average characteristic coefficients for the response of the three tested wheels plus thermocouple

Process	$\overline{\chi_1} \pm U(\overline{\chi_1})$	$\overline{\tau_1} \pm U(\overline{\tau_1})$ (s)	$\overline{\chi_2} \pm U(\overline{\chi_2})$	$\overline{\tau_2} \pm U(\overline{\tau_2})$ (s)
Wheel MS-100 plus thermocouple (V_{air} = 1.6 m/s)				
Heating	0.83 ± 0.03	22 ± 2	0.17 ± 0.03	177 ± 76
Cooling	0.81 ± 0.02	20 ± 1	0.19 ± 0.02	144 ± 3
Wheel SG-150 plus thermocouple (V_{air} = 0.8 m/s)				
Heating	0.76 ± 0.02	46 ± 3	0.24 ± 0.02	290 ± 38
Cooling	0.75 ± 0.05	48 ± 8	0.25 ± 0.05	248 ± 50
Wheel MS-200 plus thermocouple (V_{air} = 1.6 m/s)				
Heating	0.82 ± 0.05	36 ± 3	0.18 ± 0.05	226 ± 43
Cooling	0.79 ± 0.04	31 ± 2	0.21 ± 0.04	187 ± 32

are for the wheel plus humidity sensor and the wheel plus thermocouple. However, the transient response characteristics of the wheels alone are desired. Ref. [4] presents the analysis and final equations that are required to determine the corrected energy wheel humidity response using correlation equations for both the humidity sensor alone and the sensor downstream of the wheel when both are correlated using Eqs. (1) and (2). The analysis is the same to determine the thermal response of the energy wheel alone from the measured characteristics of the thermocouple alone and the thermocouple plus energy wheel [14]. This deconvolution analysis is not presented here, but the resulting response curves of the sensor, wheel plus sensor and wheel alone are contained in Fig. 5 for the 100-mm thick molecular sieve wheel.

Fig. 5(a) shows the transient response of the humidity sensor alone, wheel plus humidity sensor and wheel alone following a step increase and decrease in inlet humidity for Wheel MS-100. Fig. 5(b) contains the same for the thermocouple following a step increase or decrease in inlet temperature for Wheel MS-100. It is seen that the wheel response alone lies between the sensor response and the wheel plus sensor response for both

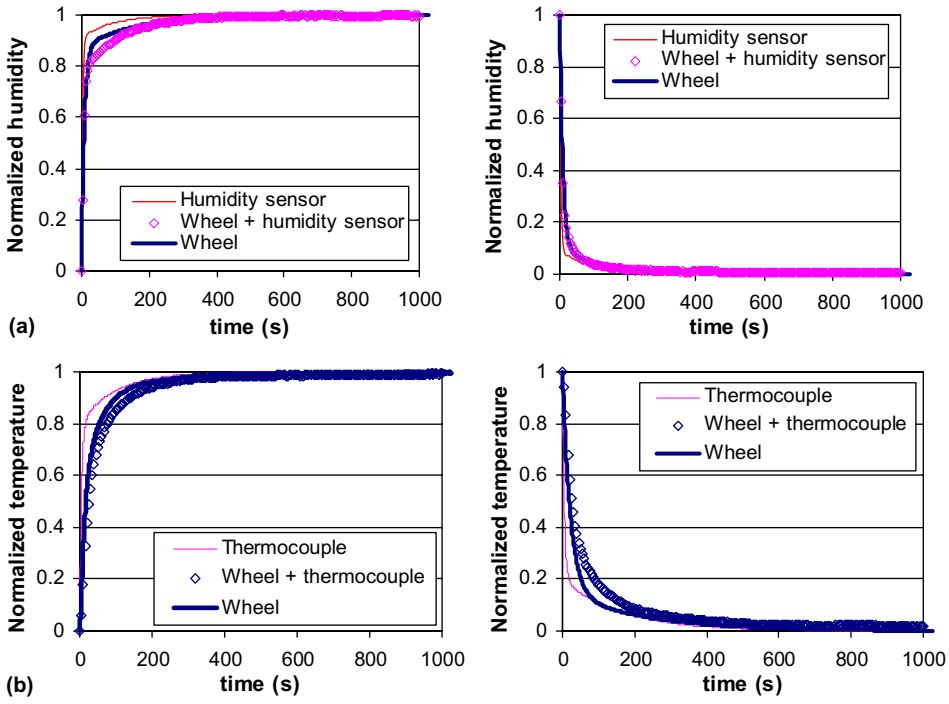

Fig. 5. (a) Normalized humidity of humidity sensor, Wheel MS-100 plus humidity sensor and Wheel MS-100 alone for a step increase and decrease in humidity and (b) normalized temperature of thermocouple, Wheel MS-100 plus thermocouple and Wheel MS-100 alone for step increase and decrease in temperature.

temperature and humidity changes. The wheel response alone is very close to the wheel plus sensor response. This confirms that the response of the wheel is not greatly altered when a humidity sensor or thermocouple sensor with a fast response is used to measure the wheel response as reported by [4,14].

Curve fitting the transient response curve of the wheel alone using Eqs. (1) and (2) gives the characteristic coefficients representing the transient humidity response and transient temperature response of the wheel alone. These coefficients are presented in Tables 5 and 6 for Wheel MS-100. It can be seen that these time constants and weighting factors are very close to those listed in Tables 1 and 3 which confirms that the sensors (humidity and thermocouple) respond quite quickly. Thus there is only a small change in the transient response of the wheel alone compared to the response of the wheel plus sensor [4].

Table 7 lists the statistically averaged transient thermal and moisture characteristics of wheels MS-100, SG-150 and MS-200. At the same face velocity, the thicker the wheel, the larger the time constants. In addition, uncertainty analysis was performed according to [19] using the 95% confidence limits. The uncertainties in the characteristic coefficients are thus included in the data presented in Table 7. The characteristic properties of the wheels presented in this table will be used later to determine the effectiveness of these wheels using the analysis presented in Part I of this paper [1].

3.4. Transient response from numerical simulations

Refs. [20,21] developed a numerical model to predict the latent and sensible effectiveness of rotary energy exchangers for different wheel designs and operating conditions. They validated their numerical results by comparing them with experimental data with known uncertainties. In this section, the numerical model of [20,21] is used to generate transient response data for energy wheels subjected to a step change in humidity (20–80% RH) at a constant temperature of 22 °C and a step change in temperature (20–40 °C) at a constant relative humidity of 5% RH. These responses are determined at three different air face velocities of 1.6, 0.8 and 0.3 m/s. The wheel investigated here has zeolite desiccant coated on an aluminium matrix. The wheel thickness is 100 mm and the wheel is designed to operate at 20 rpm. The effect of different amounts of desiccant is studied. For simplicity and clear reference, these wheels will be referred to as Wheels 5% D, 10% D and 20% D for the wheel with 0.05 kg/kg of desiccant on the wheel matrix, 0.1 kg/kg of desiccant and 0.2 kg/kg of desiccant respectively. This numerical investigation represents a test for quality control of the amount of desiccant on the wheel quoted by an energy wheel manufacturer. Energy wheels typically contain about 20% desiccant by mass, but this may vary between wheels and batches of manufactured wheels. A wheel that has less desiccant is expected to have a lower performance when compared with a wheel that

Table 5
Water vapour adsorption and desorption coefficients (χ_1, χ_2) and time constants (τ_1, τ_2) in Eqs. (1) and (2) for Wheel MS-100 alone with $\Delta RH \neq 0$, $\Delta T = 0$, $V_{air} = 1.6$ m/s for three different humidity step sizes

Inlet conditions	χ_1	τ_1 (s)	χ_2	τ_2 (s)	r^2
Adsorption (Eq. (1))					
Dry side: $T_{i,d} \approx 23$ °C, $\phi_{i,d} \approx 5\%$	0.87	8.2	0.13	146.3	0.999
Wet side: $T_{i,w} \approx 23$ °C, $\phi_{i,w} \approx 40\%$	0.89	11.0	0.11	167.9	0.999
	0.90	11.9	0.10	179.5	0.999
Dry side: $T_{i,d} \approx 23$ °C, $\phi_{i,d} \approx 5\%$	0.82	7.8	0.18	146.0	0.999
Wet side: $T_{i,w} \approx 23$ °C, $\phi_{i,w} \approx 50\%$	0.83	10.6	0.17	168.7	0.999
	0.90	6.7	0.10	134.9	0.999
Dry side: $T_{i,d} \approx 23$ °C, $\phi_{i,d} \approx 5\%$	0.86	9.6	0.14	152.1	0.999
Wet side: $T_{i,w} \approx 23$ °C, $\phi_{i,w} \approx 60\%$	0.88	6.9	0.12	125.8	0.999
	0.85	9.3	0.15	141.8	0.999
Desorption (Eq. (2))					
Dry side: $T_{i,d} \approx 23$ °C, $\phi_{i,d} \approx 5\%$	0.91	9.1	0.09	141.2	0.999
Wet side: $T_{i,w} \approx 23$ °C, $\phi_{i,w} \approx 40\%$	0.89	7.3	0.11	112.7	0.999
	0.91	8.3	0.09	135.1	0.999
Dry side: $T_{i,d} \approx 23$ °C, $\phi_{i,d} \approx 5\%$	0.92	9.5	0.08	181.8	0.999
Wet side: $T_{i,w} \approx 23$ °C, $\phi_{i,w} \approx 50\%$	0.90	7.2	0.1	126.5	0.999
	0.89	7.2	0.11	90.1	0.999
Dry side: $T_{i,d} \approx 23$ °C, $\phi_{i,d} \approx 5\%$	0.90	6.1	0.1	100.5	0.999
Wet side: $T_{i,w} \approx 23$ °C, $\phi_{i,w} \approx 60\%$	0.92	7.8	0.08	128.7	0.999
	0.90	6.3	0.1	103.8	0.999

Table 6
Heat transfer heating and cooling coefficients (χ_1, χ_2) and time constants (τ_1, τ_2) in Eqs. (1) and (2) for Wheel MS-100 alone with $\Delta RH = 0$, $\Delta T \neq 0$, V_{air}=1.6 m/s for two different temperature step sizes

Inlet conditions	χ_1	τ_1 (s)	χ_2	τ_2 (s)	r^2
Temperature increase (Eq. (1))					
Hot side: $T_{i,d} \approx 23$ °C, $\phi_{i,d} \approx 4\%$	0.91	24.8	0.09	505.7	0.999
Cold side: $T_{i,w} \approx 53$ °C, $\phi_{i,w} \approx 4\%$	0.91	20.0	0.09	141.3	0.999
	0.88	20.5	0.12	148.7	0.999
	0.91	21.8	0.09	174.3	0.999
	0.91	22.6	0.09	265.4	0.999
Hot side: $T_{i,d} \approx 23$ °C, $\phi_{i,d} \approx 4\%$	0.91	21.6	0.09	229.2	0.999
Cold side: $T_{i,w} \approx 44$ °C, $\phi_{i,w} \approx 4\%$	0.86	19.9	0.14	128.9	0.999
	0.87	19.8	0.13	131.2	0.999
	0.88	19.6	0.12	115.5	0.999
Temperature decrease (Eq. (2))					
Hot side: $T_{i,d} \approx 23$ °C, $\phi_{i,d} \approx 4\%$	0.84	21.9	0.16	159.4	0.999
Cold side: $T_{i,w} \approx 53$ °C, $\phi_{i,w} \approx 4\%$	0.85	21.9	0.15	221.0	0.999
	0.78	20.5	0.22	116.4	0.999
	0.80	20.1	0.20	137.3	0.999
	0.82	21.3	0.18	138.2	0.999
Hot side: $T_{i,d} \approx 23$ °C, $\phi_{i,d} \approx 4\%$	0.79	19.0	0.21	126.0	0.999
Cold side: $T_{i,w} \approx 44$ °C, $\phi_{i,w} \approx 4\%$	0.80	20.1	0.20	120.9	0.999
	0.76	19.1	0.24	108.3	0.999
	0.80	21.1	0.20	105.6	0.999

Table 7
Humidity and temperature transient characteristic properties of Wheels MS-100, SG-150 and MS-200 (wheel alone)

Wheel	$\overline{\chi_1} \pm U(\overline{\chi_1})$	$\overline{\tau_1} \pm U(\overline{\tau_1})$ (s)	$\overline{\chi_2} \pm U(\overline{\chi_2})$	$\overline{\tau_2} \pm U(\overline{\tau_2})$ (s)
Humidity response				
MS-100 ($V_{air} = 1.6$ m/s)	0.89 ± 0.02	8.4 ± 1.0	0.11 ± 0.02	138 ± 17
SG-150 ($V_{air} = 0.8$ m/s)	0.91 ± 0.02	16.2 ± 2.4	0.09 ± 0.02	296 ± 49
MS-200 ($V_{air} = 1.6$ m/s)	0.79 ± 0.02	15.1 ± 1.8	0.21 ± 0.02	151 ± 26
Temperature response				
MS-100 ($V_{air} = 1.6$ m/s)	0.87 ± 0.02	20.7 ± 1.2	0.13 ± 0.02	171 ± 59
SG-150 ($V_{air} = 0.8$ m/s)	0.80 ± 0.02	45.7 ± 5.6	0.20 ± 0.02	220 ± 32
MS-200 ($V_{air} = 1.6$ m/s)	0.83 ± 0.04	32.2 ± 2.4	0.17 ± 0.04	218 ± 43

has more desiccant. This investigation tests whether the new transient model could be used to determine if different batches of energy wheels manufactured by the same manufacturer have the same amount of desiccant.

To determine the time constants of these simulated wheels, the simulated data are normalized relative to the maximum change obtained in the simulated data and the data correlated with an exponential function as in Eq. (1) and (2). The transient simulated responses are found to result in good correlations with one-time constant, which means that $\chi_1 = 1$ and $\chi_2 = 0$. Table 8 presents the average response characteristics of these wheels during adsorption and desorption, and heating and cooling. Also included in the table are the uncertainties, determined from the standard deviation of the curve fitting of the simulated response data using commercial software and correlation Eqs. (1) and (2). Table 8 shows that Wheel 20% D with the largest amount of desiccant has the largest time constants at all flow rates, especially during the humidity response test. This is expected because the greater the amount of desiccant on each wheel, the greater the moisture storage capacity and thus the slower the wheel responds to changes in the inlet conditions. It is also observed that, as the face velocity decreases, the time constants increase for all the wheels. This is because a decrease in the air face velocity reduces the rate of advection heat and moisture transfer and hence the outlet temperature and humidity will respond slower to a change in the inlet conditions. The characteristic properties listed in Table 8 will be used in the next section to determine the latent and sensible effectiveness of these wheels.

Table 8
Humidity and temperature transient characteristic properties (time constants) of wheels with 5%, 10% and 20% desiccant by mass fraction at face velocities $V_{air} = 1.6$, 0.8, 0.3 m/s

Face velocity (m/s)	Humidity response			Temperature response		
	$\bar{\tau} \pm U(\bar{\tau})$ (s)			$\bar{\tau} \pm U(\bar{\tau})$ (s)		
	Wheel 5% D	Wheel 10% D	Wheel 20% D	Wheel 5% D	Wheel 10% D	Wheel 20% D
1.6	2.1 ± 0.2	6.2 ± 0.5	14.2 ± 1.2	10.3 ± 0.9	10.3 ± 0.1	11.4 ± 0.9
0.8	5.2 ± 0.4	22.2 ± 2.1	30.1 ± 2.8	18.9 ± 1.6	19.1 ± 2.0	20.2 ± 1.9
0.3	13.9 ± 1.1	36.4 ± 3.8	80.3 ± 9.5	85.9 ± 10.1	85.9 ± 10.1	88.1 ± 10.3

4. Effectiveness results and verification with steady state tests

The effectiveness and uncertainty results for Wheels MS-100, SG-150, MS-200, 5% D, 10% D and 20% D are presented in this section. These results are calculated using the statistically averaged time constants and weighting factors presented in Tables 7 and 8 in the transient effectiveness model presented in Part I of this paper [1]. Wheels MS-100, SG-150 and MS-200 have been previously tested using the standard steady state test method in [2,3] and therefore these wheels allow the transient method to be validated. Wheels 5% D, 10% D and 20% D are wheels whose steady state effectiveness values have been determined using a validated numerical model [20,21]. All steady state effectiveness values are determined at both ARI summer and winter test conditions [2]. These test conditions are 35 °C, 47.5% RH (hot side) and 23.9 °C, 51.5% RH (cold side) for summer conditions and 21.1 °C, 48.1% RH (hot side) and 1.7 °C, 82.1% RH (cold side) for winter conditions. The results obtained from this new transient effectiveness model are compared with the known steady state effectiveness values for the wheels to verify the accuracy of the new method.

4.1. Steady state standard tests

Fig. 6 compares the latent and sensible effectiveness and their uncertainties obtained from the new transient effectiveness model [1] (Part I) with the results obtained from the steady state standard tests for Wheels MS-100, SG-150 and MS-200. For steady state standard tests, the uncertainty in the latent and sensible effectiveness should not exceed ±7% and ±5% respectively [22]. For the transient tests, the uncertainty in latent and sensible effectiveness are found to be about ±5% and ±4% which are slightly better than the standard steady state test method. The comparison in Fig. 6 shows that the results obtained from the transient test method agree, within the uncertainty bounds, with the results obtained from the steady state experimental method. This demonstrates the accuracy of the transient test method. As seen in Table 2, Wheel MS-100 which was tested at a face velocity of 1.6 m/s, has the smallest time constant of all the three wheels because it has the lowest moisture transfer area; thus the effectiveness is the lowest. Wheel SG-150 has a longer time constant because it is determined at a face velocity of 0.8 m/s and also has a higher moisture transfer area (i.e., 150-mm thick wheel) and silica gel coating. Wheel MS-200, with a thickness of 200 mm, has the largest moisture transfer area with a molecular sieve coating but the time constant is determined at a face velocity of 1.6 m/s and the effectiveness is measured at

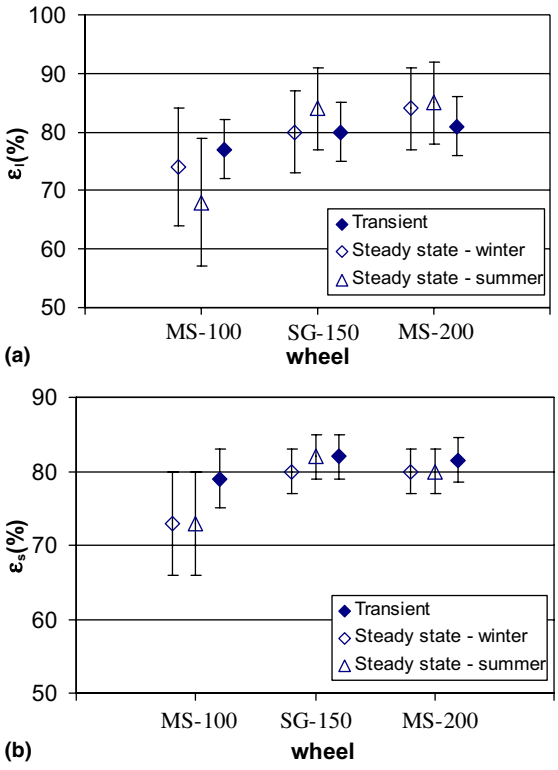

Fig. 6. Comparison of the (a) latent and (b) sensible effectiveness and uncertainty obtained from the new effectiveness model (transient) and the steady state standard tests for Wheels MS-100 ($V_{air} = 1.6$ m/s, $w = 20$ rpm), SG-150 ($V_{air} = 0.8$ m/s, $w = 20$ rpm) and MS-200 ($V_{air} = 1.6$ m/s, $w = 16$ rpm) at ARI winter and summer test conditions.

16 rpm compared to 0.8 m/s and 20 rpm for wheel SG-100. As a result of these factors, the performance of wheel MS-200 is only slightly higher than Wheel SG-150. In addition, it must be noted that the effect of using the characteristics of the wheels plus sensors to calculate the effectiveness (rather than the deconvoluted characteristics of the wheel alone) only results in ±1% error. This shows that the response characteristics of the sensors will not cause any significant error on the predicted effectiveness of the wheels if the response characteristics of the wheels plus sensors are used to predict the effectiveness for the case of fast responding sensors as used in this paper.

It should be noted that since the transient results predicted are the same for ARI summer and winter test conditions, perhaps only one test condition is needed to quantify effectiveness. Also the steady state effectiveness determined at ARI summer and winter test conditions show close agreement suggesting ARI may want to alter their test conditions to minimize the uncertainty in the effectiveness.

4.2. Steady state numerical simulations

Fig. 7 shows the comparison of the latent and sensible effectivenesses obtained from the new effectiveness model with the results obtained from the numerical simulations for Wheels 5% D, 10% D and 20% D. These results show that as the face velocities decrease, the effectiveness increases. The results can be explained because NTU is inversely proportional to the face velocity; so

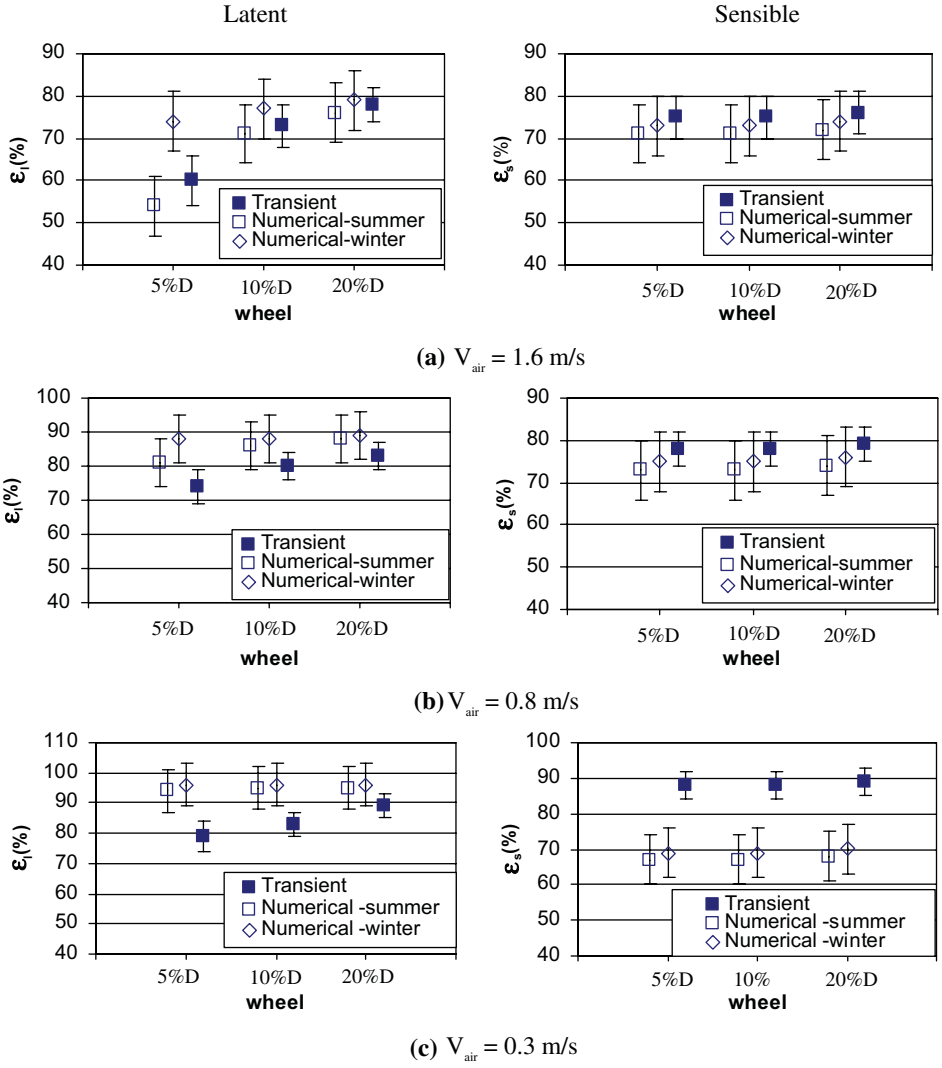

Fig. 7. Comparison of the latent (ε_l) and sensible (ε_s) effectiveness and uncertainty obtained from the new effectiveness model and the steady state numerical simulations for Wheels 5% D, 10% D and 20% D at ARI winter and summer conditions.

that as the face velocity reduces, NTU increases (Eq. (5) of Part I of this paper [1]). Thus, the effectiveness, which depends directly on NTU, is seen to increase as the face velocity decreases.

The agreement between the new effectiveness model and the simulation is within the uncertainty bounds for all wheels when the face velocity is 1.6 and 0.8 m/s. There is, however, a lack of agreement for Wheels 5% D and 10% D for a face velocity of 0.3 m/s as shown in Fig. 7(c). It must be noted that at this small face velocity of 0.3 m/s, the numerical simulation results obtained for Wheels 5% D and 10% D could not be verified experimentally because there is no practical way to remove desiccant from the wheel to result in a desiccant coating mass fraction of a half or quarter of the typical value of 20% by mass. This investigation was meant to be a sensitivity study, which, if practical, could be used as test for quality control for the amount of desiccant on the wheel quoted by an energy wheel manufacturer. Wheels 5% D and 10% D, which have a matrix desiccant mass fractions of quarter and half respectively, have less desiccant to enhance moisture transfer in the wheel compared to Wheel 20% D with full desiccant mass fraction.

Despite, the poorer agreement between steady state and transient methods shown in Fig. 7(c), both methods show a decrease in effectiveness as the mass fraction of desiccant decreases. This indicates that the transient method and facility could be used as a quality control tool to compare different batches of energy wheels from the same manufacturer to ensure that the amount of desiccant has not changed. The transient method also correctly shows that the effectiveness increases as the face velocity decreases, which is well known in heat exchange design and is predicted by the simulation model for all cases except for effectiveness at the lowest face velocity. The simulated sensible effectiveness at $V_{air} = 0.3$ m/s (Fig. 7(c)) are lower than the simulated sensible effectiveness at $V_{air} = 0.8$ and 1.6 m/s (Fig. 7(a) and (b)). The simulated results include corrections for axial heat conduction in the matrix, but the equations used in Part I of this paper [1] neglect this effect. Latent effectiveness is not affected by axial diffusion and therefore the latent is inversely related to the face velocity for both methods. In Fig. 7(c), the numerical simulation shows that as the face velocity is reduced to a low value (i.e., 0.3 m/s), the latent effectiveness increases, but the sensible effectiveness reduces. This difference between sensible and latent effectiveness is not accounted for in the new (transient) effectiveness model which depends only on the humidity and temperature time constants which are measured independently, and the speed of the wheel alone. In addition, at very low wheel speeds and face velocities, the axial heat conduction is important and has significant effects on the sensible effectiveness of the wheel. However, axial heat conduction is not of great importance at the face velocities typically used in HVAC systems (i.e., 1.5–4 m/s) and therefore this limitation of the new transient test method is not a serious limitation for practical applications. In addition, the effect of axial conduction is likely to be different for parallel flow and counter flow heat exchangers and the model does not consider this.

5. Conclusions

The analytical model presented in Part I of this paper [1], for predicting the effectiveness of a counter flow energy wheel from transient measurements, has been compared with steady state experimental standard test data and steady state numerical simulations. Using a previously developed test facility, the time constants of several different wheels were measured. At same face velocity, the thicker the wheel, the larger the time constants. Sensible and latent effectivenesses, calculated from the new analytical model using these measured time constants, show agreement within uncertainty bounds with the effectivenesses obtained from standard steady state tests and with few exceptions, with the effectiveness calculated with a validated numerical model. Since the new test method is faster, more versatile (applicable for field testing and manufacturing plant quality control), requires less expensive equipment and is slightly more accurate than the standard steady state test method, it is expected to have wide applications.

Acknowledgements

Financial assistance from the Natural Sciences and Engineering Research Council of Canada (NSERC), Venmar CES, Saskatoon and the Canada Foundation for Innovation (CFI) are greatly appreciated.

References

[1] O.O. Abe, C.J. Simonson, R.W. Besant and W. Shang, Effectiveness of energy wheels from transient measurements: Part I—Prediction of effectiveness and uncertainty, Int. J. Heat Mass Transfer in press, doi:10.1016/j.ijheatmasstransfer.2005.08.002.

[2] ARI Standard 1060–2003, Rating Air-to-Air Energy Recovery Equipment American Refrigeration Institute, Arlington, 2003.

[3] ASHRAE Standard 84–1991, Method of Testing Air-to-Air Heat Exchangers, American Society of Heating, Refrigerating and Air Conditioning Engineers Inc., Atlanta, 1991.

[4] Y.H. Wang, C.J. Simonson, R.W. Besant, W. Shang, Transient humidity measurements and characteristics for humidity sensors and energy wheels, ASHRAE Trans. 111 (2) (2005) 353–369.

[5] J.A. Clark, V.S. Arpaci, K.M. Treadwell, Dynamic response of heat exchangers having internal heat sources—Part I, Trans. ASME 80 (1958) 612–624.
[6] F.E. Romie, Transient response of the counter flow heat exchanger, J. Heat Transfer 106 (3) (1984) 620–626.
[7] F.E. Romie, Transient response of the parallel flow heat exchanger, J. Heat Transfer 107 (3) (1985) 727–730.
[8] M. Lachi, N.E. Wakil, J. Padet, The time constant of double pipe and one pass shell-and-tube heat exchangers in the case of varying flow rates, Int. J. Heat Mass Transfer 40 (9) (1997) 2067–2079.
[9] J. Yin, M.K. Jensen, Analytical model for transient heat exchanger response, Int. J. Heat Mass Transfer 46 (2003) 3255–3264.
[10] R.I. Loehrke, Evaluating the results of the single-blow transient heat exchanger test, Exp. Thermal Fluid Sci. 3 (6) (1990) 574–580.
[11] X. Luo, W. Roetzel, U. Ludersen, The single-blow transient testing technique considering longitudinal core conduction and fluid dispersion, Int. J. Heat Mass Transfer 44 (2001) 121–129.
[12] X. Luo, U. Ludersen, The single-blow transient testing technique for plate-fin heat exchangers, Int. J. Heat Mass Transfer 44 (2001) 3745–3753.
[13] W. Shang, Evaluation of energy wheel performance, Ph.D. thesis, University of Saskatchewan, Saskatoon, 2002.
[14] Y.H. Wang, Transient characteristics of humidity sensors and their application to energy wheels, MSc. thesis, University of Saskatchewan, Saskatoon, 2005. Available from: <http://library.usask.ca/theses/available/etd-04052005-223929/unrestricted/ETD.pdf>.
[15] O.O. Abe, Y.H. Wang, C.J. Simonson, R.W. Besant, W. Shang, Transient temperature measurements and characteristics for temperature sensors and energy wheels, ASHRAE Trans. 112 (2) (2005), submitted for publication.
[16] O.O. Abe, Effectiveness of energy wheels from transient measurements, MSc. thesis, University of Saskatchewan, Saskatoon, 2005.
[17] J.R. Taylor, An Introduction to Error Analysis—The Study of Uncertainties in Physical Measurements, University Science Books, California, 1982, pp. 147–152.
[18] J.W. Rizika, Thermal lags in flowing system containing heat capacitors, Trans. ASME 76 (1954) 411–420.
[19] ASME PTC 19.1, Test Uncertainty, American Society of Mechanical Engineers, New York, 1998.
[20] C.J. Simonson, R.W. Besant, Heat and moisture transfer in desiccant coated rotary energy exchangers: Part I—numerical model, Int. J. HVAC&R Res. 3 (4) (1997) 325–350.
[21] C.J. Simonson, R.W. Besant, Heat and moisture transfer in desiccant coated rotary energy exchangers: Part II—validation and sensitivity studies, Int. J. HVAC&R Res. 3 (4) (1997) 351–368.
[22] D.L. Ciepliski, C.J. Simonson, R.W. Besant, Some recommendations for improvements to ASHRAE Standard 84–1991, ASHRAE Trans. 104 (1B) (1998) 1651–1965.